An optical diagnostics investigation on the effect of pilot injection dwell time and injection pressure on combustion characteristics and soot emissions in a single-cylinder optical diesel engine

Yannis Hardalupas[1], Christopher Hong[2], Christos Keramiotis[3], Alex M.K.P. Taylor[4], Dimitios Touloupis[5] and Georgios Vourliotakis[6]

Abstract

The present work investigates the effect of the injection dwell time and injection pressure on soot reduction potential in an optical single cylinder light duty diesel engine. The engine operated under a double injection scheme, under low load and low engine speed conditions. The conducted experiments considered two different dwell times for three different injection pressures. The fuel quantity of the main injection was adjusted to maintain the same IMEP value among all cases considered. Findings were analysed *via* means of pressure trace and apparent heat release rate (AHRR) analyses, as well as a series of optical diagnostics techniques, namely high-speed imaging and planar Laser Induced Incandescence (pLII). The combination of dwell time and injection pressure substantially affects charge reactivity and soot oxidation potential. The analysis suggests that a shorter dwell time, combined with a higher injection pressure, can lead to an enhanced potential for engine-out particulate reduction, by creating an in-cylinder environment, which promotes soot oxidation. Overall, results indicate that a close coupled pilot and main injection scheme can reduce soot levels, while, however, increasing specific fuel consumption by up to 12% to maintain the same engine power output levels.

Keywords

[1]Professor, Dept. of Mechanical Engineering, Imperial College London, SW7 2AZ London, UK. E-mail: y.hardalupas@imperial.ac.uk
[2]Research Associate, Dept. of Mechanical Engineering, Imperial College London, SW7 2AZ London, UK. E-mail: christopher.hong03@imperial.ac.uk
[3]Research Associate, Dept. of Mechanical Engineering, Imperial College London, SW7 2AZ London, UK. E-mail: c.keramiotis@imperial.ac.uk
[4]Professor, Dept. of Mechanical Engineering, Imperial College London, SW7 2AZ London, UK. E-mail: a.m.taylor@imperial.ac.uk
[5]Research Associate, Dept. of Mechanical Engineering, Imperial College London, SW7 2AZ London, UK (corresponding author). E-mail: d.touloupis@imperial.ac.uk

Introduction

Engine technology is evolving in response to increasingly stringent emissions limits imposed by regulations across the world (*e.g.* Johnson, 2015). Emission legislation prescribes limits to both emitted particulate mass and particle number. Understanding the in-cylinder soot oxidation processes may help to lead to strategies, which reduce engine-out particulate emissions, which would have significantly beneficial effects not only on fuel economy, air quality and human health, but also with respect to minimization of the need for after treatment in production vehicles (*e.g.* Li, Guan, Luo, & Huang, 2015). Soot production in a diesel engine can be correlated to the ratio of the durations of premixed-burn to diffusion-burn (or mixing controlled) phases, with the diffusion regime being responsible for a greater portion of the soot produced. Higher temperatures and higher local equivalence ratio (Φ) inside the cylinder should be avoided, otherwise some of the injected fuel will locally form fuel rich "pockets" among the charge, prone to soot formation (*e.g.* Koci et al., 2009). A Partially Premixed Combustion (PPC) operation mode may in principle exhibit suitable fuel/air mixing, limiting the formation of conditions susceptible to soot formation and thus has the potential to lead to reduced soot emissions (*e.g.* Musculus, Miles, & Pickett, 2013).

Multiple injection patterns can be employed under a PPC operation mode, since the lower in-cylinder temperature during the pre-injection events does not lead to auto-ignition of the pilot fuel, and thus the desired fuel-air mixture stratification can be achieved. In the literature, splitting a single fuel injection into two or more subsequent injection events has been identified as an effective means for reducing engine particulate emissions. Early experiments in single cylinder metal engines (*e.g.* Nehmer & Reitz, 1994) suggest that for a double injection scheme *per* cycle, there is an optimal pilot fuel quantity for reducing the engine-out particulate emissions and that a shorter dwell time could lead to lower Brake Specific Fuel

Consumption (BSFC). However, no apparent correlation between the dwell time and particulate emissions was found.

Following those early experiments, and in an effort to understand the governing mechanism behind the reduction of particulates when using multiple injections, numerical methods were employed (*e.g.* Han, Uludogan, G. Hampson, & Reitz, 1996; Patterson, Kong, Hampson, & Reitz, 1994). The computations revealed that during a single injection event, fuel rich regions form at the spray tip, which are the main source of soot formation. During a multiple injection event, however, those fuel rich areas are not present, the mixture becomes leaner and more stratified and soot formation weakens.

In an effort to study experimentally the physics behind the effect of multiple injection events on combustion, various experiments have been conducted using constant volume chambers (*e.g.* Amagai, Hashimoto, & Arai, 1999; Zhang, Ito, & Nishida, 2001; Zhang & Nishida, 2004). The aforementioned experiments reveal that a well-tuned double injection, in terms of dwell time, could shorten the ignition delay, by altering the fuel evaporation rate inside the chamber. They also showed that the amount of premixed combustion could be controlled by the dwell time and the amount of injected fuel in the first injection, as long as it is below 25 percent of the total fuel injected, *per* cycle.

Furthermore, experiments conducted in either "metal" or optical engines outlined a number of effects associated with double injection schemes (*e.g.* Busch et al., 2015; Ehleskog, Ochoterena, & Andersson, 2007; Koyanagi, Öing, Renner, & Maly, 1999; Lee & Reitz, 2003). One of the most important effects of pilot injection, and the reason why it is commonly exploited in production engines, is the combustion noise suppression caused by the shorter ignition delay and the lower heat release peak, due to the premixed combustion mode.

Many experimental studies have also focused on the effect of double injection schemes on emission reduction (*e.g.* Gill, Marriner, Sison, & Zhao, 2005; Liu & Reitz, 2005; Ogawa & Miyamoto, 2000; Vanegas, Won, Felsch, Gauding, & Peters, 2008; Yang & Chung, 2013). Chen, (2000) used a 4-cylinder engine to study the effect of multiple injections on NO_x and particulate emissions. The results showed that for light duty diesel engines, the use of a small amount of pilot fuel injection (less than 1.0 mg/ stroke) leads to simultaneous NO_x and soot emission reduction, with the appropriate combination of EGR rates and injection timings. Beatrice, Belardini, Bertoli, Lisbona, & Migliaccio, (2001) used one metal and one optical engine, equipped with the same cylinder head, to study various multiple injection schemes. They concluded that the interaction between pilot and main injection fuel jets is highly complex, requiring further investigation. However, they mention that the optimum dwell angle between the pilot and the main injection events appears to be a strong controlling factor for emission reduction. Further investigation of this topic on an optical engine by Beatrice, Belardini, Bertoli, Lisbona, & Rossi Sebastiano, (2002) suggests that the main controlling factor of air-fuel mixing with the use of a double injection scheme is the swirl motion of the charge inside the cylinder. When a double injection scheme is utilized, the swirling gas flow removes the combustion products from the region of first pulse during the dwell time before the second pulse is injected. However, if the dwell is too long, the products of the first pulse can be transferred into the region of the second pulse. Therefore, proper tuning of the dwell time is necessary for soot emission control. Subsequent studies by Ehleskog & Ochoterena, (2008) and Yao Mingfa, Wang Hu, Zheng Zunqing, & Yue Yan, (2009) agree on the potential of soot reduction with the use of double injection schemes, because of improved air utilization that promotes soot oxidation. However, they observed no clear relationship between dwell time and net soot production.

The present work attempts to assess the effects of injection pressure and dwell time between two subsequent injections on soot production and its evolution inside the bore of a single cylinder optical diesel engine and, ultimately, the potential for reduction of engine-out particulate emissions. The assessment is attempted *via* means of in-cylinder pressure trace analysis, high-speed imaging of flame natural luminosity and planar Laser Induced Incandescence (pLII).

Experimental Setup and Methodology

The engine utilized for this experimental campaign was an optical Ricardo Hydra single cylinder low duty diesel engine (93.62 mm bore; 90.55 mm stroke; 623 cm^3 displacement; 16.9 geometric compression ratio), equipped with a Ford York I4 2.5 lt engine cylinder head and a common rail fuel injection system (8-holes injectors, with 140° cone angle). The engine configuration and the associated instrumentation have been described in detail recently (Founti et al. 2015; Hong 2015). The engine features a metal piston with an optical window in the piston crown and, in the liner, a metal annulus that accommodates insets for four optical windows. In-cylinder pressure trace is acquired with a Kistler 6056A41 Quartz Pressure Sensor (logged at every 0.2 CAD) and the analysis of the recorded signal was realized using in-house developed codes to calculate the apparent heat release rate (using the Woschni correlation for the heat release model; *e.g.* (Woschni and Fieger 1979)). The codes also calculate and apply corrections for the thermodynamic loss angle, which is the crank angle difference between the physical top dead centre (TDC) and the crank angle where peak motoring pressure occurs. For all cases, the coefficient of variation for the IMEP was found to be less than 2% when 50 consecutive cycles were measured.

A Photron Fastcam APX-RS high-speed CMOS camera imaged the high-speed chemiluminescence and flame natural luminosity, controlled by LaVision HighSpeed Controller, equipped with a 105 mm (1:1.8) UV Nikon lens. The camera acquired data at a frequency of 10 kHz, which corresponds approximately to 3 images *per* 2 CAD at 1200 rpm engine speed. The exposure time of the recorded images was 100 μs and the resolution was 512x512 pixels. The image acquisition took place for 10 consecutive cycles, with 100 images *per* cycle. The optical filters used for natural luminosity imaging were two WG395 high transmissivity filters (Edmund optics) to cut out the ultraviolet wavelengths, for the CH^* chemiluminescence a 430 nm bandpass filter (FWHM 20 nm, T_{max}=45%) was used, whereas the chemiluminescence from C_2^* was passed through an optical bandpass filter at 514 nm (FWHM 30 nm, T_{max}=54%). OH^* imaging was realized *via* combining a FGUV11S (Thorlabs, FWHM 30 nm, T_{max}=82%) coloured glass filter and a WG295 high transmissivity filter (Edmund optics).

For the qualitative planar Laser Induced Incandescence (pLII) measurements, the laser used for exciting the soot particles was a Quanta-Ray Pro 270-10Hz laser, operating at 532 nm wavelength, with 900 mJ of energy *per* pulse and pulse width of 1-2 ns. The laser beam was guided into the combustion chamber using appropriate mirrors compatible with this specific wavelength and was transformed into a focused laser sheet using a series of cylindrical lenses from Thorlabs with focal lengths of -50 mm, 150 mm and 1000 mm. The laser sheet passed through two of the side windows of the combustion annulus, thereby crossing the bore and was terminated by a beam dump. Due to the size and the positioning of the optical windows, the laser sheet had a width of approximately 5 mm. Due to limitations in the optical access, pLII measurements of the soot remaining after the post-injection pulses were obtained at 31 CAD and 50 CAD aTDC. A LaVision FlowMaster 3S fitted with an intensifier and a 105 mm (1:1.8) UV Nikon lens was used to capture the pLII signal through a Samrock FF01-

405/10-25 filter that had a centre wavelength of 405 nm with guaranteed minimum bandwidth of 10nm, which filtered out most of the chemiluminescence and other fluorescence signals. The final images presented here are a result of intensity thresholding to remove noise caused by the intensifier, and averaging over 100 consecutive cycles.

The findings of the experimental campaign are discussed on the basis of both optical measurements and *via* pressure trace and apparent rate of heat release analyses. The use of chemiluminescence in engine studies is a useful diagnostic tool for local measurements of combustion characteristics (*e.g.* Aleiferis, Hardalupas, Taylor, Ishii, & Urata, 2004; Hardalupas & Orain, 2004). Each of the chemiluminescent species is a proxy of a fundamental combustion property. OH^* has been found to be a good proxy of the heat release zone and the flame lift-off location during second-stage combustion and is used to characterize spatial and temporal ignition, as well as the level of combustion stratification, which can be linked to fuel stratification prior to the auto-ignition (*e.g.* I. Najafabadi, 2017; M. I. Najafabadi et al., 2017). CH^* is related to the reaction zone and the flame front, while C_2^* is indicative of fuel-rich reactive areas. The C_2 and C_2H radicals are the precursor species for the CH^* radicals (Bozkurt et al. 2012) and are formed within a narrow reaction zone with high temperature gradients. The short-lived CH^* radicals are hence considered as a proxy for the flame front and can also be used to support arguments on the reactivity. On the other hand, CH_2 and C_3 species play a prominent role on the formation of the excited C_2^* species, which become more intense in the locally formed fuel-rich pockets. Therefore, C_2^* chemiluminescence is correlated to the reacting fuel-rich zones (*e.g.* Kohse-Höinghaus 1994; Hultqvist et al. 1999; Kathrotia et al. 2012). Flame natural luminosity from diesel combustion is useful for the study of soot, because it mainly originates from soot luminescence and incandescence. The signal from the flame natural luminosity can be correlated with the total soot oxidation rate and, within the context of the present study, is considered as a proxy of

the in-cylinder soot levels, while (broadband) luminous combustion takes place. For the detection of soot when it is no longer detectably "self-luminous", that is to say, after the completion of the luminous combustion, the signal from pLII was used.

In the present work, the employment of a PPC-like mode under low-load and low-speed conditions has been chosen, since O'Connor & Musculus, (2013) suggest that such conditions have the best potential for demonstrating the positive effects of multiple injection strategies, while using conventional fuel injection equipment as found in diesel passenger cars (Bakker et al. 2014).

Pressure trace analysis

In the present section, the thermodynamics of the combustion are analysed using the in-cylinder pressure trace and apparent rates of heat release.

Table 1 shows the operating conditions used for the experiments. The optical engine operated at a constant speed of 1200 RPM and the engine load was kept constant at approximately 2.8 bar IMEP. All the investigated cases feature a double injection scheme, consisting of a pilot and a main injection event, with the changing variables being the injection pressure and the dwell angle between the two subsequent injection events. Three different injection pressures, namely 300, 500 and 800 bar, as well as two dwell angles, 4 and 6 CAD (corresponding to 552 μs and 828 μs at 1200 rpm respectively) were investigated, resulting in a total of 6 cases. The timing of the main injection was kept constant at 2 CAD bTDC, whereas the timing of the pilot injection was set to either 6 or 8 CAD bTDC. The fuel quantity of the pilot injection was kept constant at 1mg/cycle and the fuel quantity of the main injection was adjusted in each case to maintain the same engine load levels. Figure 1 shows, indicatively, the current of

the fuel injector for two cases, with different dwell time between the injections, at 300 bar injection pressure.

Figure 2 shows the evolution of the in-cylinder pressure whereas Table 2 shows some thermodynamic characteristics of the combustion for all the cases considered. When the injection pressure increases, the peak in-cylinder pressure increases as well, from *ca.* 40 bar for Case 1 to 50 bar for Case 6, as Figure 2 shows and, as a result, the maximum pressure rise rate (PRR) increases, as shown in Table 2. This rapid increase in pressure will lead to higher combustion noise. Moreover, higher injection pressure leads overall to advanced combustion in terms of timing, as indicated by CA50 in Table 2, which is the crank location where the 50% of the total heat release has occurred. An advanced combustion event seems to favour combustion efficiency, because, for the cases where the CA50 values are between 6 and 8 CAD, namely Cases 3-6, less fuel *per* cycle is required to maintain the same levels of engine load for both dwell angles, as seen in Table 1.

The same effects as increasing the injection pressure, but less pronounced, can be observed when shortening the dwell time between the two injections. Maximum in-cylinder pressure and maximum pressure rise rate slightly increase, while combustion timing advances and combustion duration becomes shorter, especially for the 300 bar injection pressure cases, *i.e.* Cases 1 and 2. It is important to note here that with a shorter dwell time, more fuel *per* cycle is required in order to achieve the same levels of engine load, thus deteriorating the combustion efficiency.

The Cumulative Apparent Heat Release (CAHR) presented in Figure 3 can provide a better insight into the combustion process, by revealing the different phases of combustion. When the fuel is injected, the jet formed at the nozzle exit breaks up and fuel atomizes. Then, because of the high temperature environment, it vaporizes and, because of the swirl, it mixes

with the air inside the cylinder, to form a combustible mixture. This process of atomization and vaporization absorbs energy from the in-cylinder environment, which explains the initial drop in the CAHR graph (Figure 3) for all cases. When the injection pressure increases, Figure 3 shows that this drop becomes more evident, indicating better atomization of the fuel injected, leading, eventually, to better mixing of the in-cylinder charge. The drop is slightly more pronounced when the dwell time is shorter, however, the underlying cause here is different, as it will be illustrated later in the manuscript, with the analysis of the optical measurements.

The first part of the CAHR graph, after the initial drop, corresponds to the premixed phase of the combustion process and is characterized by high gradients of apparent heat release. With the increase of the injection pressure, or with shorter dwell time, the premixed phase becomes more rapid and reaches higher values of heat release in the CAHR graph, explaining the higher in-cylinder pressure and PRR values observed. Moreover, when the premixed phase of the combustion is more intense, more energy is released from the fuel earlier in terms of crank angle and so the whole combustion process advances, as indicated by the smaller values of the CA50. The diffusion part of the combustion, *i.e.* the second part of the CAHR graph characterized by smaller gradients of apparent heat release compared to the premixed phase, is shorter when the premixed phase is more intense, leading to overall shorter combustion duration, as described earlier.

Optical Measurements Analysis

In the present section, the analysis of the optical measurements takes place. The optical diagnostics used are, namely, high-speed imaging of the flame natural luminosity and C_2^* and OH^* chemiluminescence, as well as pLII for non-luminous soot detection at 31 and 50 CAD

aTDC. The analysis is performed on two axes: the effect of dwell time and the effect of injection pressure.

Dwell time

For the analysis of the effect of dwell time, we are focusing on the 300 bar injection pressure cases, *i.e.* Case 1 and 2. That is because the effect is more pronounced for lower injection pressures and a large portion of the combustion for these cases takes place at the inner part of the bore, which is optically accessible, thus providing a better understanding on the combustion process.

Figure 4 shows the spatially integrated C_2^* chemiluminescence signal for all six cases considered. The recorded signal for Case 2, *i.e.* the case with the short dwell, is lower throughout the expansion stroke, compared to Case 1. For Case 1 the signal peaks at 16 CAD, whereas, for Case 2 the signal peaks earlier, at 14.4 CAD, and the peak value for Case 2 is down by 60% when compared to the peak value recorded for Case 1. Later at the expansion stroke, this divergence between the recorded values for the two cases becomes larger, as at 31 CAD aTDC the recorded signal for Case 2 is 86% lower and at 50 CAD aTDC 96% lower. In order to get a better understanding on the spatial distribution of the fuel rich areas inside the cylinder, as depicted by the C_2^* chemiluminescence, the recorded images at the crank angle where peak integrated signal was observed for both cases are presented. Figures 5 and 6 show the average recorded image of C_2^* chemiluminescence at 16 CAD for Case 1 and 14.4 CAD for Case 2 respectively. The longer dwell between the pilot and the main injection leads to more intense fuel rich areas, which occupy a larger portion of the cylinder area, as seen in Figure 5. On the other hand, Figure 6 shows that with the shorter dwell, these fuel rich areas become less intense and limited towards the inner part of the cylinder. It is also important to note here that for the long dwell case the fuel rich areas coincide with the plumes formed by

the fuel jets during the injection, whereas for the short dwell case they appear more homogenized, losing their distinctive pattern. From the previous analysis, it can be inferred that, as soot originates from the fuel rich areas of the combustion, for the short dwell case the generation of soot inside the cylinder is reduced and becomes more spatially homogeneous, compared to the long dwell case.

Figure 7 shows the spatially integrated natural flame luminosity signal for all six cases studied. Comparing Cases 1 and 2 again, a reduction of 16% in the peak value and an average drop of 50% at the recorded signal later at the expansion stroke for Case 2 is noticed. As mentioned earlier, the natural luminosity of the flame is closely related to soot oxidation. Therefore, the conclusion that the short dwell case exhibits lower soot oxidation rates than the long dwell case can be made.

So far, the two opposing forces that affect the soot distribution inside the cylinder have been discussed: soot generation inside the fuel rich areas of the charge and soot oxidation as indicated by the intensity of the natural luminosity of the flame. For the short dwell case (Case 2), soot generation rate is vastly lower than in the long dwell case (Case 1) and could result in lower engine-out soot emissions, despite the fact that soot oxidation weakens. To get a better view on engine-out soot emissions, the pLII measurements are presented.

Figure 8 shows a juxtaposition of chemiluminescence measurements and pLII measurements for two different crank angles, namely 31 and 50 CAD for Cases 1 and 2. The high-speed measurements are superimposed using different colours: white for the natural luminosity of the flame, blue for the OH^* chemiluminescence, green for the C_2^* chemiluminescence and red for the CH^* chemiluminescence. Figure 9 shows the spatially integrated pLII signal for both crank angles and both cases.

First, it is important to note in Figure 8 that there is a strong correlation between the areas where soot is captured by the pLII and the fuel rich areas of the cylinder charge (green colour). This further supports the argument made about the soot generation from the fuel rich pockets. Interestingly, as seen in Figure 9, for the long dwell case (Case 1), the recorded pLII signal is higher at 50 CAD than at 31 CAD, implying that soot generation still surpasses soot oxidation, because of the intensified fuel rich zones. For the short dwell case (Case 2), the recorded pLII signal at 50 CAD is lower than at 31 CAD, as soot oxidation dominates over soot generation. Therefore, since soot chemistry freezes later at the expansion stroke, the short dwell case will exhibit lower engine-out soot emissions.

At this point, the effect of dwell time on combustion behaviour and the implications on soot emissions have been discussed; however, the cause of this different behaviour has not been mentioned.

Figure 10 shows a sequence of instantaneous natural luminosity images for Cases 1 and 2 at selected crank angles. The first visible auto ignition spot for Case 1 can be observed at 0.7 CAD, whereas for Case 2 appears later, at 5.8 CAD. As the first visible auto ignition spot indicates the onset of the diffusion phase of the combustion, it can be deduced that combustion in Case 1 enters the diffusion phase earlier and while the main injection is still in progress, as seen at the image corresponding to 2.2 CAD. On the contrary, combustion in Case 2 enters the diffusion phase at 5.8 CAD, very close to the end of the main injection event. This delay in the onset of the diffusion phase allows for better stratification of the in-cylinder charge, by giving the fuel of the main injection more time to mix with the rest of the charge, leading, as seen before, to enhanced premixed combustion phase and less intense, more homogeneous fuel-rich zones.

The reason for this delay of visible auto ignition in Case 2 over Case 1 can be attributed to the injection timings. In the short dwell case (Case 2) the plume of fuel vapour from the pilot injection has little time available to rotate (due to the swirling flow) away from the axis of the jet. When the main fuel is injected, the pilot fuel cools down and the visible, hot auto ignition is delayed. On the contrary, for the long dwell case (Case 1) the plume of the pilot fuel has more time available to rotate away from the jet axis and to heat up, so its capability to auto ignite remains somewhat unaffected. This argument can be supported by Figures 11 and 12, which show the average flame front at 14.4 CAD, depicted using OH^* chemiluminescence for Case 1 and 2 respectively. The flame front in Case 1 is locally confined and more intense when compared to the widely spread, weaker flame front in Case 2. This suggests that in Case 2 there is better fuel distribution and the flame front covers a larger portion of the visible area of the cylinder.

The point raised in the previous paragraph emphasizes the essence of the PPC mode. Enhanced premixing and lower charge stratification can be achieved, not only by using advanced injection timings, but also by placing the individual injection events properly.

Injection pressure

The injection pressure has significant effect on the thermodynamics of the combustion, as discussed in section 2 above, by enhancing atomization and vaporization of the fuel, thus favouring the mixing of the in-cylinder charge and the premixed phase of the combustion. In the present section, the effect of injection pressure using optical diagnostics is investigated.

In Figure 4 it is evident that the total C_2^* decreases drastically with the increase of the injection pressure. Therefore, the fuel rich areas inside the cylinder diminish and soot generation is weak. This behaviour can be attributed to the enhanced mixing caused by the increase of injection pressure; however, it should be noted that limited optical access could

affect the measurements. It is interesting to observe the peak in the C_2^* signal for the high-pressure cases with the long dwell, *i.e.* Cases 3 and 5. The peaks appear at around 15 CAD aTDC for both cases and they indicate the presence of fuel rich areas within the inner part of the cylinder, close to the injector tip. Figures 13 and 14 show indicatively the instantaneous spatially resolved C_2^* signal at 15 CAD aTDC for Cases 5 and 6 (800 bar injection pressure) respectively. The short dwell case (Case 6) exhibits lower intensity in the fuel rich areas formed close to the injector tip than the long dwell case (Case 5), indicating that the short dwell limits the generation of soot in the area around the injector tip, an area that is the main source of soot at high injection pressures.

As far as the natural luminosity of the flame is concerned, in Figure 7 it is evident that the trend, which existed at 300 bar injection pressure, is reversed for the cases featuring higher injection pressures. The SINL signal is higher for the short dwell cases (Cases 4 and 6) when compared to the respective long dwell cases (Cases 3 and 5), implying higher soot oxidation rates.

It is interesting to note that for the 800 bar injection pressure cases, *i.e.* Cases 5 and 6, the natural luminosity of the flame, whose presence indicates the diffusion phase of the combustion, appears instantly at around 10 CAD aTDC. In Figures 15 and 16, which show the instantaneous spatially resolved natural luminosity signal at 11 CAD aTDC for Cases 5 and 6 respectively, the natural luminosity signal forms a "cloud", indicating high homogeneity of the charge. There is an exception of some local spots of high natural luminosity signal, which occur because of the local fuel rich spots mentioned earlier. This instant appearance of the natural luminosity signal explains what can be observed in Figure 3, for the high-pressure cases, as a drop in the CAHR, indicating a dissociation between the premixed and the diffusion phase of the combustion.

The homogeneity of the charge at high injection pressures can be confirmed when looking at the spatially integrated signal of OH^* chemiluminescence at Figure 17. When the injection pressure increases, OH^* signal becomes weaker, as a result of the homogeneity of the charge. Again, the local fuel rich spots serve as an exception, which, due to the local stratification, produce OH^* chemiluminescence signal.

Figure 18 shows a juxtaposition of high-speed imaging measurements and pLII measurements for two different crank angles, namely 31 and 50 CAD for Cases 1 to 6. The high-speed measurements are superimposed using different colours: white for the natural luminosity of the flame, blue for the OH^* chemiluminescence, green for the C_2^* chemiluminescence and red for the CH^* chemiluminescence. Figure 19 shows the spatially integrated pLII signal for both crank angles and all cases considered.

In Figure 19, the trend between the injection pressure and the soot formation is clear. High injection pressure leads to low levels of soot, late at the expansion stroke and, arguably, at the exhaust. This is a result of weak soot formation, combined with intense soot oxidation, as demonstrated earlier.

In Figure 18, it becomes evident that, for the 800 bar injection pressure cases, *i.e.* Cases 5 and 6, the distribution of soot at 31 CAD aTDC is mainly attributed to the fuel rich spots close to the injector tip, as it has been previously discussed. At 50 CAD aTDC soot particles can only be observed at the lip of the bowl and the integrated pLII signal intensity is lower than it was at 31 CAD aTDC. It should be noted here that the 500 bar cases, *i.e.* Cases 3 and 4, seem to be the intermediate step between the low pressure and the high-pressure cases, when it comes to soot distribution and signal intensity.

Summary and conclusions

The effect of the injection dwell time (*i.e.* the time between two subsequent injection events) and injection pressure on soot reduction potential was experimentally investigated in an optical, single cylinder, light duty diesel engine, operated in PPC mode under low load (2.8 bar IMEP) and low speed (1200 RPM) conditions. Results are deduced *via* a combination of in-cylinder pressure trace analysis, spectroscopic chemiluminescence measurements and LII signal at selected CAD. (In particular, the diverse combustion patterns are visualized by means of high-speed imaging of flame natural luminosity and CH^*, C_2^* and OH^* chemiluminescence, while planar LII experiments at 31 and 50 CAD aTDC indicate the soot concentration at the given piston position. As a result, a magnitude of evidence regarding soot oxidation rates, fuel rich areas and oxidation zones is captured.)

Results indicate that the competition between soot generation and soot oxidation is the determinant factor for the engine-out soot emissions. As soot is being generated in the fuel rich areas of the cylinder, as depicted by the C_2^* chemiluminescence, better mixing inside the cylinder creates less fuel rich areas, thus, weak soot generation. Both parameters, *i.e.* the dwell time and the injection pressure, affect the mixing process, but the dominant mechanism behind each one of them is different. A short dwell time causes longer delay for the first hot spot at the fuel injected during the pilot injection to appear, because of the cooling induced by the fuel injected during the main injection. A longer delay provides the charge with more time to mix, thus enhancing the mixing process and the premixed phase of the combustion, while supressing the diffusion phase. An increased injection pressure enhances the atomization and vaporization of the fuel, which, in combination with the in-cylinder flow, enhances the pre-mixing of the charge. In this case, too, the premixed phase of the combustion is pronounced, while the diffusion phase is supressed.

In both cases, then, soot formation weakens, while, as observed in the flame natural luminosity signal evolution, soot oxidation remains at the same order of magnitude. This leads to a reduction in the non-luminous soot levels, detected using the pLII technique, late at the expansion stroke. Consequently, the case with the high injection pressure and the short dwell exhibits the lowest levels of detected soot and, presumably, the lowest engine out soot emissions amongst all cases considered.

To conclude, the present work shows that better premixing and lower charge stratification can be achieved, not only by using advanced injection timings, but also by placing the individual injection events properly.

Acknowledgments

Nomenclature

AHRR   Apparent Heat Release Rate
aTDC   after Top Dead Centre
BSFC   Brake Specific Fuel Consumption
bTDC   before Top Dead Centre

CA50	Crank Angle where 50% of heat release has occurred
CAD	Crank Angle Degree
CAHR	Cumulative Apparent Heat Release
CMOS	Complementary Metal-Oxide Semiconductor
EGR	Exhaust Gas Recirculation
FWHM	Full Width at Half Maximum
IMEP	Indicated Mean Effective Pressure
NOx	Nitrous Oxides
pLII	planar Laser Induced Incandescence
PPC	Partially Premixed Combustion
PRR	Pressure Rise Rate
RPM	Rotations Per Minute
SINL	Spatially Integrated Natural Luminosity
TDC	Top Dead Centre
UV	Ultra-Violet

References

Aleiferis, P. G., Hardalupas, Y., Taylor, A. M. K. P., Ishii, K., and Urata, Y. (2004). "Flame chemiluminescence studies of cyclic combustion variations and air-to-fuel ratio of the reacting mixture in a lean-burn stratified-charge spark-ignition engine." *Combustion and Flame*, 136(1–2), 72–90.

Amagai, K., Hashimoto, Y., and Arai, M. (1999). "Ignition and combustion characteristics of two-stage injection diesel spray." 20, 1–5.

Bakker, P. C., De Abreu Goes, J. E., Somers, L. M. T., and Johansson, B. H. (2014). "Characterization of low load PPC operation using RON70 fuels." *SAE Technical Papers*, 1.

Beatrice, C., Belardini, P., Bertoli, C., Lisbona, M. G., and Migliaccio, M. N. (2001). "Combustion patterns in common rail D.I. Engines inferred by experiments and C.F.D.

Computations." *Combustion Science and Technology*, 162(1–6), 235–261.

Beatrice, C., Belardini, P., Bertoli, C., Lisbona, M. G., and Rossi Sebastiano, G. M. (2002). "Diesel Combustion control in common rail engines by new injection strategies." *International Journal of Engine Research*, 3(1), 23–36.

Bozkurt, M., Fikri, M., and Schulz, C. (2012). "Investigation of the kinetics of OH* and CH* chemiluminescence in hydrocarbon oxidation behind reflected shock waves." *Applied Physics B: Lasers and Optics*, 107(3), 515–527.

Busch, S., Zha, K., Miles, P. C., Warey, A., Pesce, F., Peterson, R., and Vassallo, A. (2015). "Experimental and Numerical Investigations of Close-Coupled Pilot Injections to Reduce Combustion Noise in a Small-Bore Diesel Engine." *SAE Int. J. Engines*, 8(2), 660–678.

Chen, S. K. (2000). "Simultaneous Reduction of NOx and Particulate Emissions by Using Multiple Injections in a Small Diesel Engine." *SAE Technical Paper 2000-01-3084*, (724).

Ehleskog, R., and Ochoterena, R. L. (2008). "Soot Evolution in Multiple Injection Diesel Flames." *SAE Technical Paper*, (724).

Ehleskog, R., Ochoterena, R. L., and Andersson, S. (2007). "Effects of Multiple Injections on Engine-Out Emission Levels Including Particulate Mass from an HSDI Diesel Engine." *SAE paper 2010-01-0612*, 2007(724), 2007-01–0910.

Founti, M., Hardalupas, Y., Hong, C., Keramiotis, C., Ramaswamy, K. G., Soulopoulos, N., Taylor, A., Touloupis, D. P., and Vourliotakis, G. (2015). "An Experimental Investigation on the Effect of Diluent Addition on Flame Characteristics in a Single Cylinder Optical Diesel Engine." *SAE Technical Papers*, 2015–Septe(x), 1–6.

Gill, K., Marriner, C., Sison, K., and Zhao, H. (2005). "In-cylinder Studies of Multiple Diesel Fuel Injection in a Single Cylinder Optical Engine Reprinted From : Compression

Ignition Combustion Processes 2005." 2005(724).

Han, Z., Uludogan, a, G. Hampson, and Reitz, R. (1996). "Mechanism of Soot and NOx Emission Reduction Using Multiple-injection in a Diesel Engine." *SAE Technical Paper series*, 960633(412).

Hardalupas, Y., and Orain, M. (2004). "Local measurements of the time-dependent heat release rate and equivalence ratio using chemiluminescent emission from a flame." *Combustion and Flame*, 139(3), 188–207.

Hong, C. K. H. (2015). "Laser Induced Incandescence and High Speed Imaging in Hydra Optical Diesel Engine."

Hultqvist, A., Christensen, M., Johansson, B., Franke, A., Richter, M., and Aldén, M. (1999). "A Study of the Homogeneous Charge Compression Ignition Combustion Process by Chemiluminescence Imaging." *SAE Paper 1999-01-3680*.

Johnson, T. (2015). "Engine Efficiency and Emissions Trends."

Kathrotia, T., Riedel, U., Seipel, A., Moshammer, K., and Brockhinke, A. (2012). "Experimental and numerical study of chemiluminescent species in low-pressure flames." *Applied Physics B: Lasers and Optics*, 107(3), 571–584.

Koci, C. P., Ra, Y., Krieger, R., Andrie, M., Foster, D. E., Siewert, R. M., and Durrett, R. P. (2009). "Multiple-Event Fuel Injection Investigations in a Highly-Dilute Diesel Low Temperature Combustion Regime." *SAE International Journal of Engines*, 2(1), 837–857.

Kohse-Höinghaus, K. (1994). "Laser techniques for the quantitative detection of reactive intermediates in combustion systems." *Progress in Energy and Combustion Science*.

Koyanagi, K., Öing, H., Renner, G., and Maly, R. (1999). "Optimizing Common Rail-Injection by Optical Diagnostics in a Transparent Production Type Diesel Engine." *SAE Technical Paper 1999-01-3646*, (724).

Lee, T., and Reitz, R. D. (2003). "The Effects of Split Injection and Swirl on a HSDI Diesel Engine Equipped with a Common Rail Injection System." *SAE paper*, 2003(724), 2003-01–0349.

Li, X., Guan, C., Luo, Y., and Huang, Z. (2015). "Effect of multiple-injection strategies on diesel engine exhaust particle size and nanostructure." *Journal of Aerosol Science*, 89, 69–76.

Liu, Y., and Reitz, R. D. (2005). "Optimizing HSDI Diesel Combustion and Emissions Using Multiple Injection Strategies." 2005(724).

Musculus, M. P. B., Miles, P. C., and Pickett, L. M. (2013). *Conceptual models for partially premixed low-temperature diesel combustion. Progress in Energy and Combustion Science*, Elsevier Ltd.

Najafabadi, I. (2017). *Optical study of stratification for partially premixed combustion Optical Study of Stratification for M . Izadi Najafabadi*.

Najafabadi, M. I., Egelmeers, L., Somers, B., Deen, N., Johansson, B., and Dam, N. (2017). "The influence of charge stratification on the spectral signature of partially premixed combustion in a light-duty optical engine." *Applied Physics B: Lasers and Optics*, Springer Berlin Heidelberg, 123(4), 1–13.

Nehmer, D. a, and Reitz, R. D. (1994). "Measurement of the Effect of Injection Rate and Split Injections on Diesel Engine Soot and NOx Emissions." *SAE Technical paper*, (940668), 1–14.

O'Connor, J., and Musculus, M. P. B. (2013). "Post Injections for Soot Reduction in Diesel Engines: A Review of Current Understanding." *SAE Int. J. Engines*, 6(1), 400–421.

Ogawa, H., and Miyamoto, N. (2000). "Improvements of diesel combustion and emissions with two-stage fuel injection at different piston positions." *SAE Technical Paper*, (724).

Patterson, M. A., Kong, S.-C., Hampson, G. J., and Reitz, R. D. (1994). "Modeling the

Effects of Fuel Injection Characteristics on Diesel Engine Soot and NOx Emissions." *SAE Technical Paper*, 940523(940523).

Vanegas, A., Won, H., Felsch, C., Gauding, M., and Peters, N. (2008). "Experimental Investigation of the Effect of Multiple Injections on Pollutant Formation in a Common-Rail DI Diesel Engine." 2008(724).

Woschni, G., and Fieger, J. (1979). "DETERMINATION OF LOCAL HEAT TRANSFER COEFFICIENTS AT THE PISTON OF A HIGH SPEED DIESEL ENGINE BY EVALUATION OF MEASURED TEMPERATURE DISTRIBUTION." *SAE Paper*.

Yang, S. Y., and Chung, S. H. (2013). "An experimental Study on the Effects of High-Pressure and Multiple Injection Strategies on DI Diesel Engine Emissions." *Fuel*, 78(x), 1303–1317.

Yao Mingfa, Wang Hu, Zheng Zunqing, and Yue Yan. (2009). "Experimental Study of Multiple Injections and Coupling Effects of Multi-Injection and EGR in a HD Diesel Engine." *SAE Techcnical Paper*, 4970(2009-01–2807).

Zhang, Y., Ito, T., and Nishida, K. (2001). "Characterization of Mixture Formation in Split-Injection Diesel Sprays via Laser Absorption- Scattering (LAS) Technique." *Sae Paper 2001-01-3498*, (724).

Zhang, Y., and Nishida, K. (2004). "Effect of Injection Temporal Splitting on the Characteristics of Fuel-air Mixture Formation in a Common Rail Diesel Spray." *Proceedings of the Institution of Mechanical Engineers, Part D: Journal of Automobile Engineering*, IMECHE, 218(3), 323–331.

Table 1. Injection schedule details for all cases considered. Engine speed at 1200 RPM and engine load at 2.8 car IMEP in all cases.

Case no.	Injection Pressure (bar)	Pilot Injection Timing//Quantity (CAD aTDC //mg)	Main Injection Timing//Quantity (CAD aTDC //mg)
1	300	-8//1	-2//17
2	300	-6//1	-2//17.6
3	500	-8//1	-2//15.2
4	500	-6//1	-2//17.2
5	800	-8//1	-2//15
6	800	-6//1	-2//17

Table 2. Global combustion characteristics for all cases considered in the present work.

Case no.	IMEP (bar)	Max Pressure (bar)	Max PRR (bar/CAD)	CA50 (CAD)	CA90-CA10 (CAD)
1	2.8	39.9	4.1	10.8	29.8
2	2.8	41.2	5.0	10.4	28.8
3	2.8	44.0	5.4	7.6	28.2
4	2.8	44.7	6.0	7.9	28.7
5	2.8	49.6	8.2	6.4	25.9
6	2.8	49.8	8.5	6.5	25.3

Fig. 1. Definition of dwell angle between two subsequent injection events within the same engine cycle, based on the current of the injector.
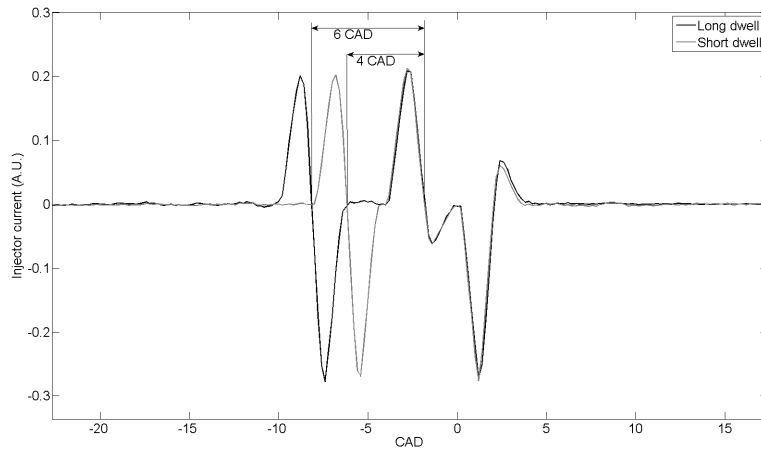
Fig. 2. Measured in-cylinder pressure as a function of crank angle degrees for all cases considered.
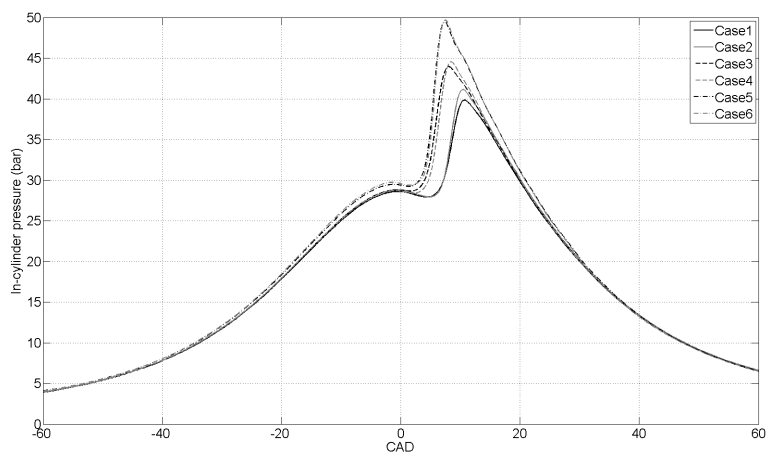
Fig. 3. Cumulative apparent heat release as a function of crank angle for all cases considered.
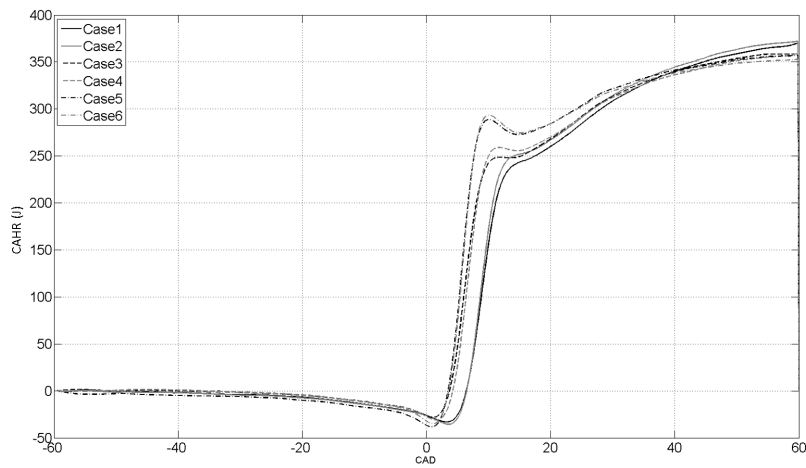
Fig. 4. Spatially integrated C_2^* chemiluminescence signal as a function of crank angle for all cases considered.
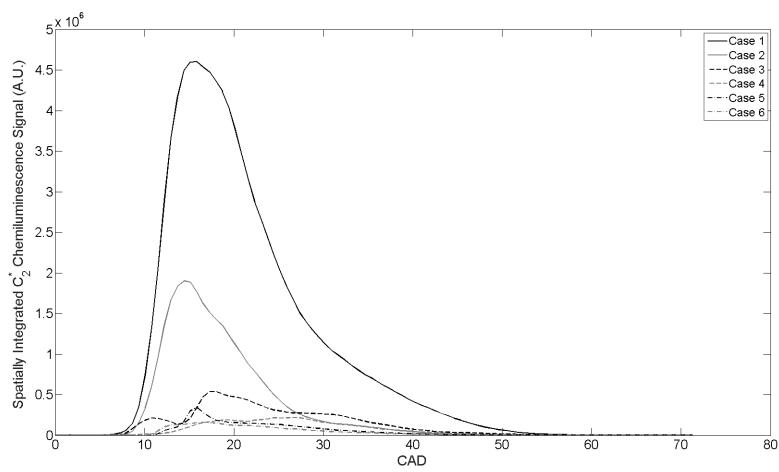
Fig. 5. Average spatially resolved C_2^* chemiluminescence signal at 16 CAD aTDC for Case 1.
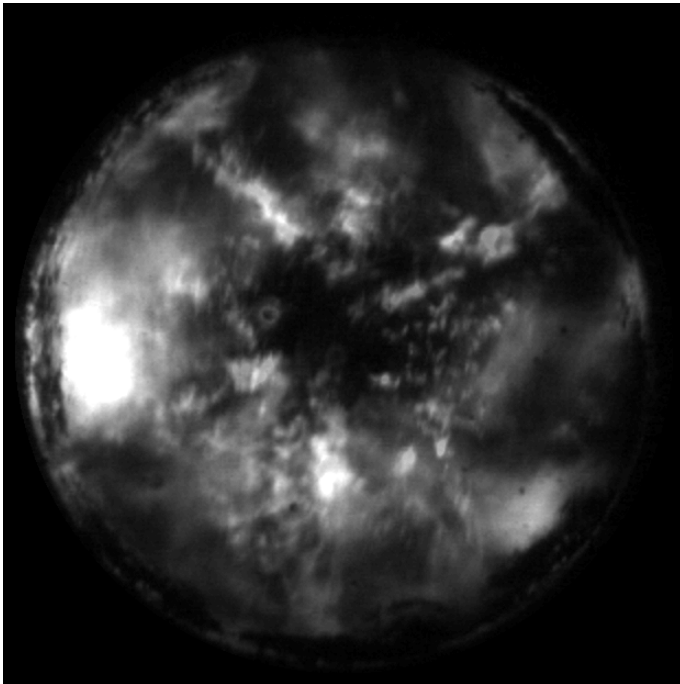
Fig. 6. Average spatially resolved C_2^* chemiluminescence signal at 14.4 CAD aTDC for Case 2.
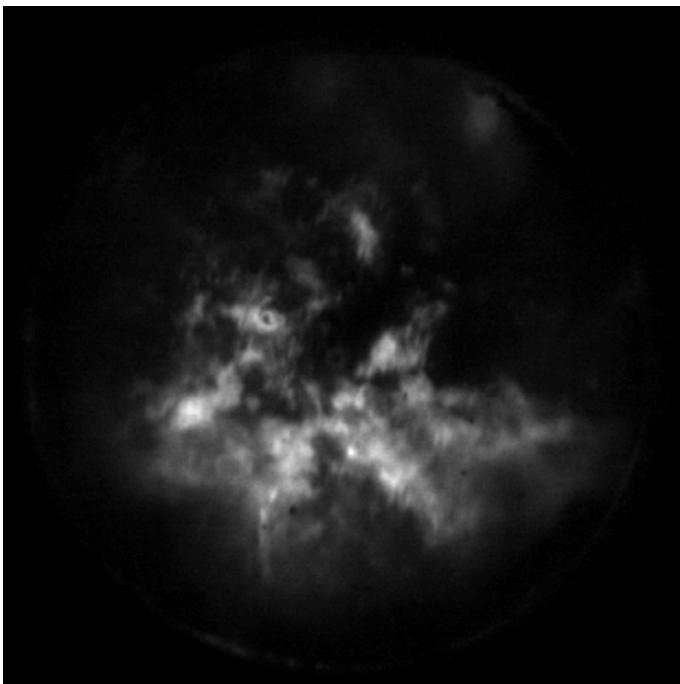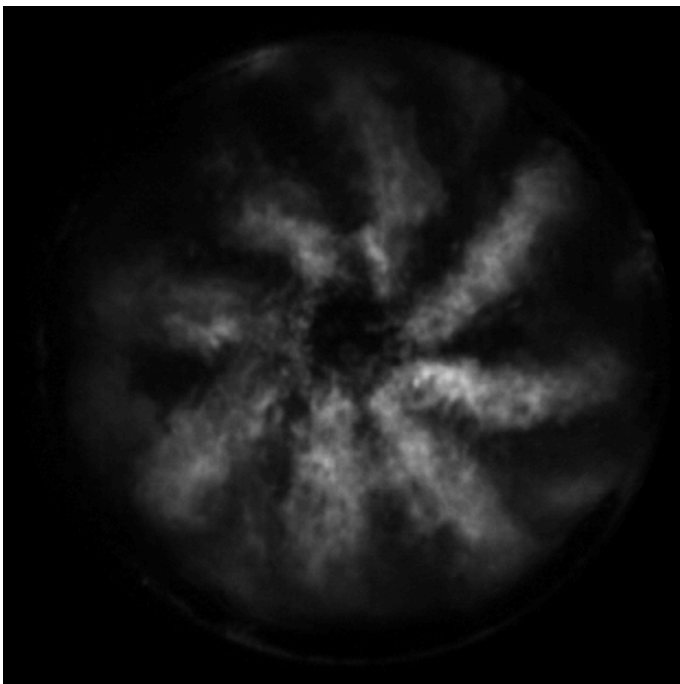
Fig. 7. Spatially integrated natural luminescence signal as a function of crank angle for all cases considered.
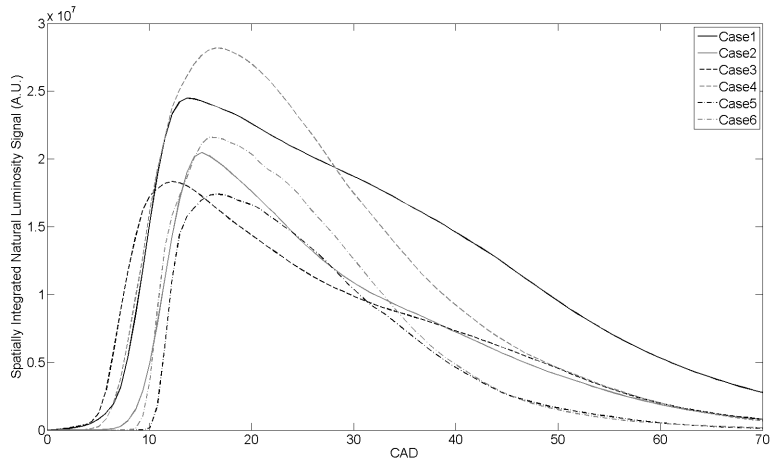
Fig. 8. Upper row: Superimposed average images of flame spectroscopic measurements with natural luminosity (white), OH* chemiluminescence (blue), CH* chemiluminescence (red) and C$_2$* chemiluminescence (green) and, lower row, the corresponding planar LII imaging measurements at 31 (upper frame) and 50 CAD aTDC (lower frame).
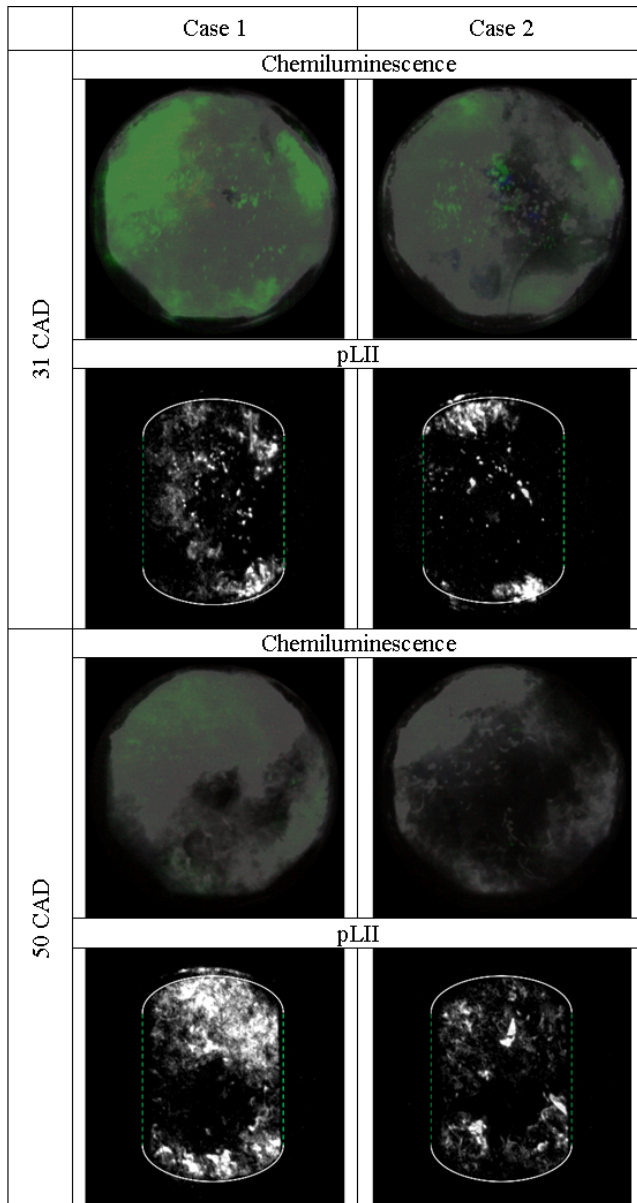
Fig. 9. Spatially integrated pLII signal for Cases 1 and 2 at 31 and 50 CAD aTDC.
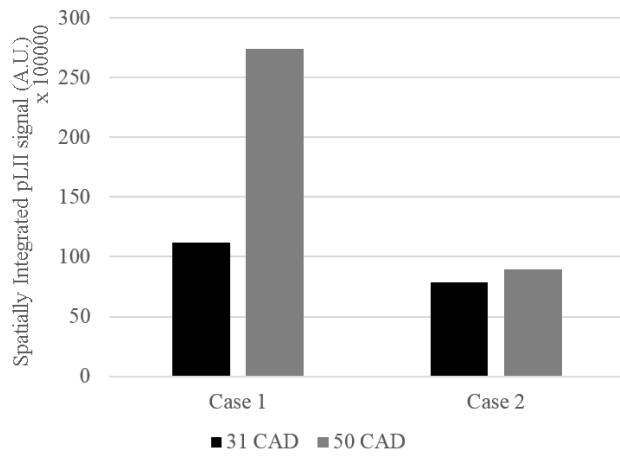
Fig. 10. Instantaneous Natural Luminosity images at selected CAD for Cases 1 and 2
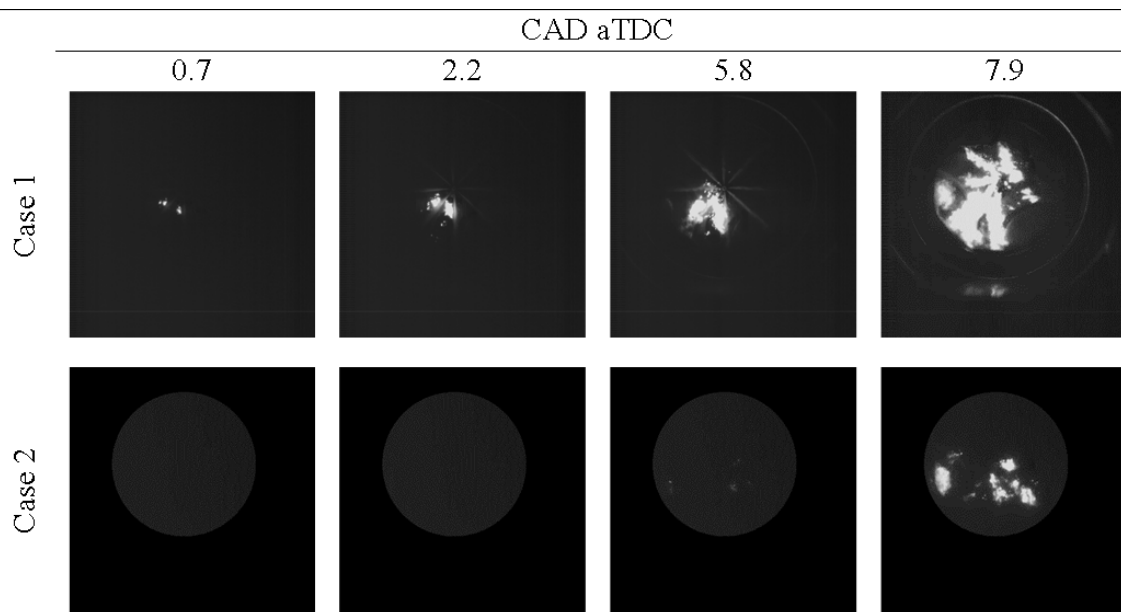
Fig. 11. Average spatially resolved OH* chemiluminescence signal at 14.4 CAD aTDC for Case 1.
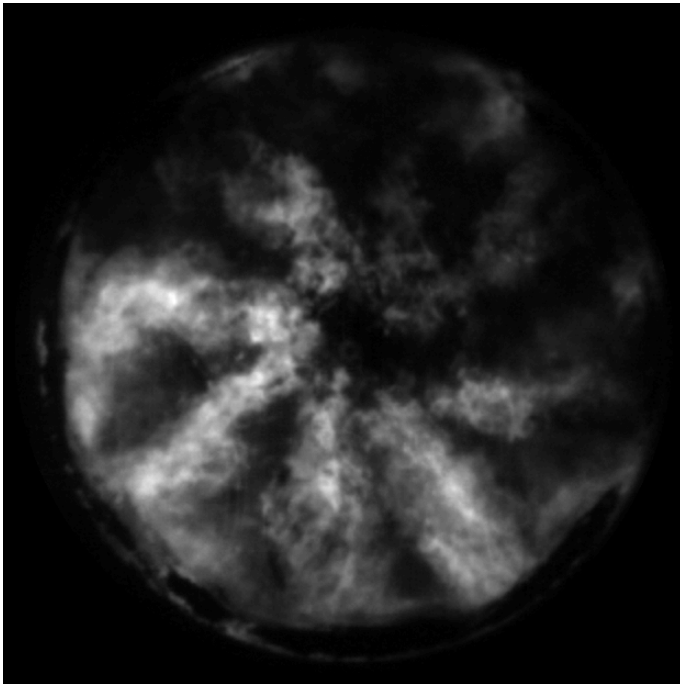
Fig. 12. Average spatially resolved OH* chemiluminescence signal at 14.4 CAD aTDC for Case 2.

Fig. 13. Instantaneous spatially resolved C_2^* signal at 15 CAD aTDC for Case 5.
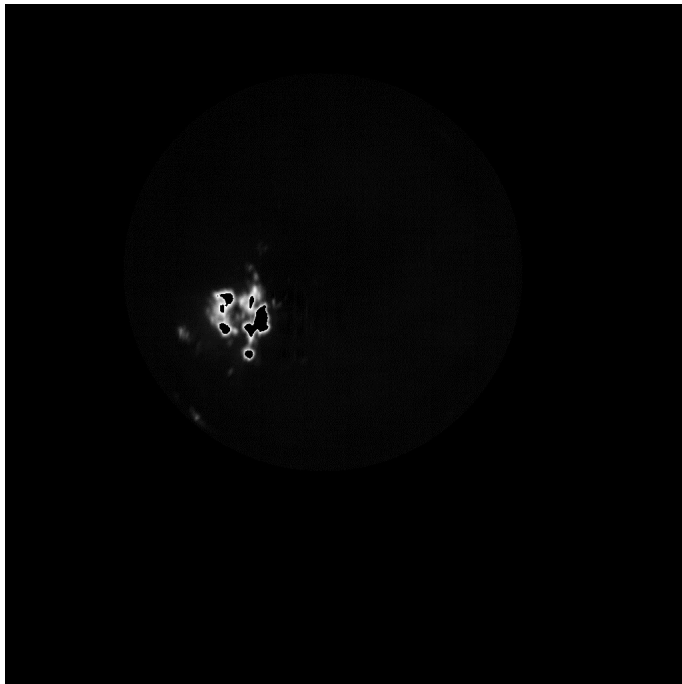
Fig. 14. Instantaneous spatially resolved C_2^* signal at 15 CAD aTDC for Case 6.
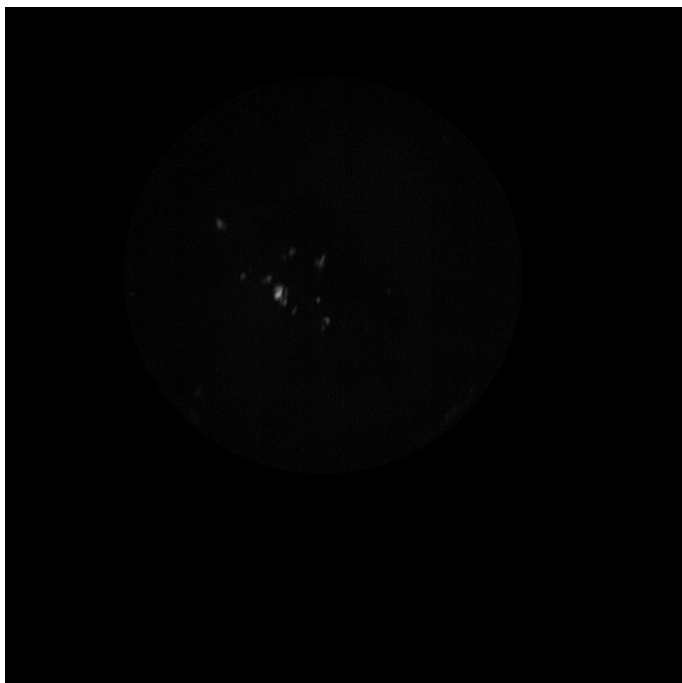
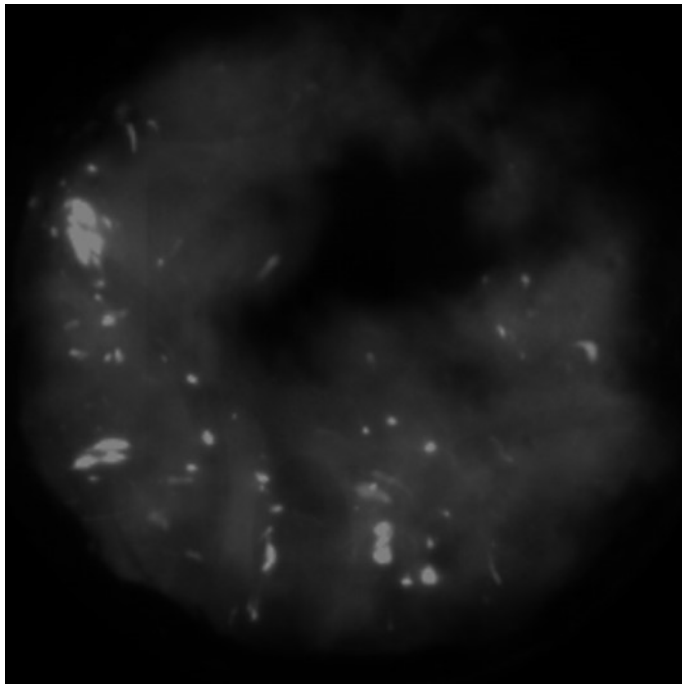**Fig. 15.** Average spatially resolved Natural Luminosity signal at 11 CAD aTDC for Case 5.

Fig. 16. Average spatially resolved Natural Luminosity signal at 11 CAD aTDC for Case 6.
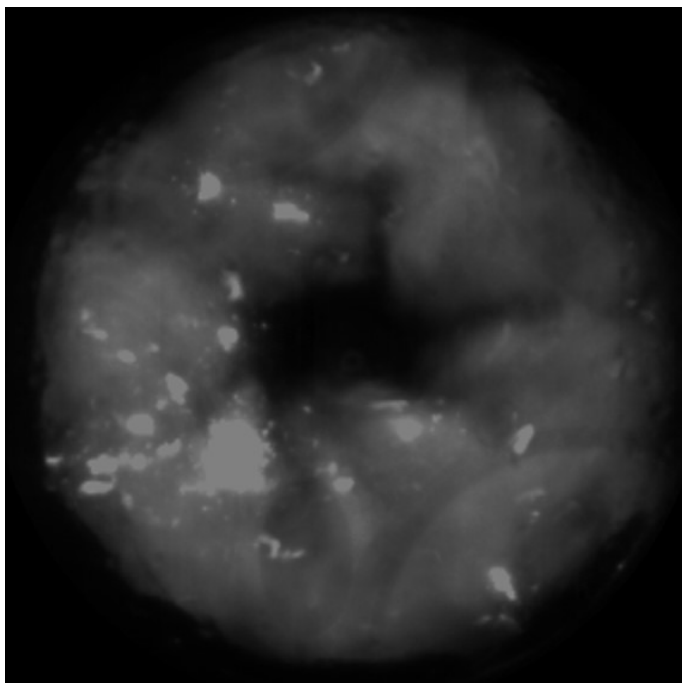
Fig. 17. Spatially integrated OH* signal as a function of crank angle for all cases considered.
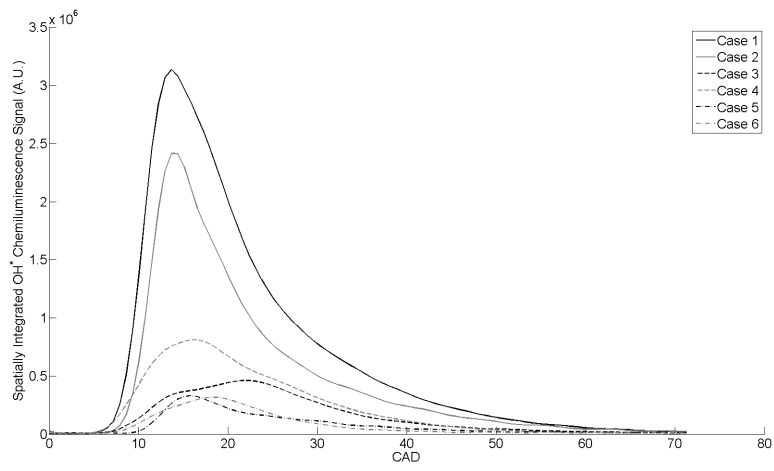
Fig. 18. Upper row: Superimposed average images of flame spectroscopic measurements with natural luminosity (white), OH* chemiluminescence (blue), CH* chemiluminescence (red) and C$_2$* chemiluminescence (green) and, lower row: the corresponding planar LII imaging measurements at 31 (upper frame) and 50 CAD aTDC (lower frame).
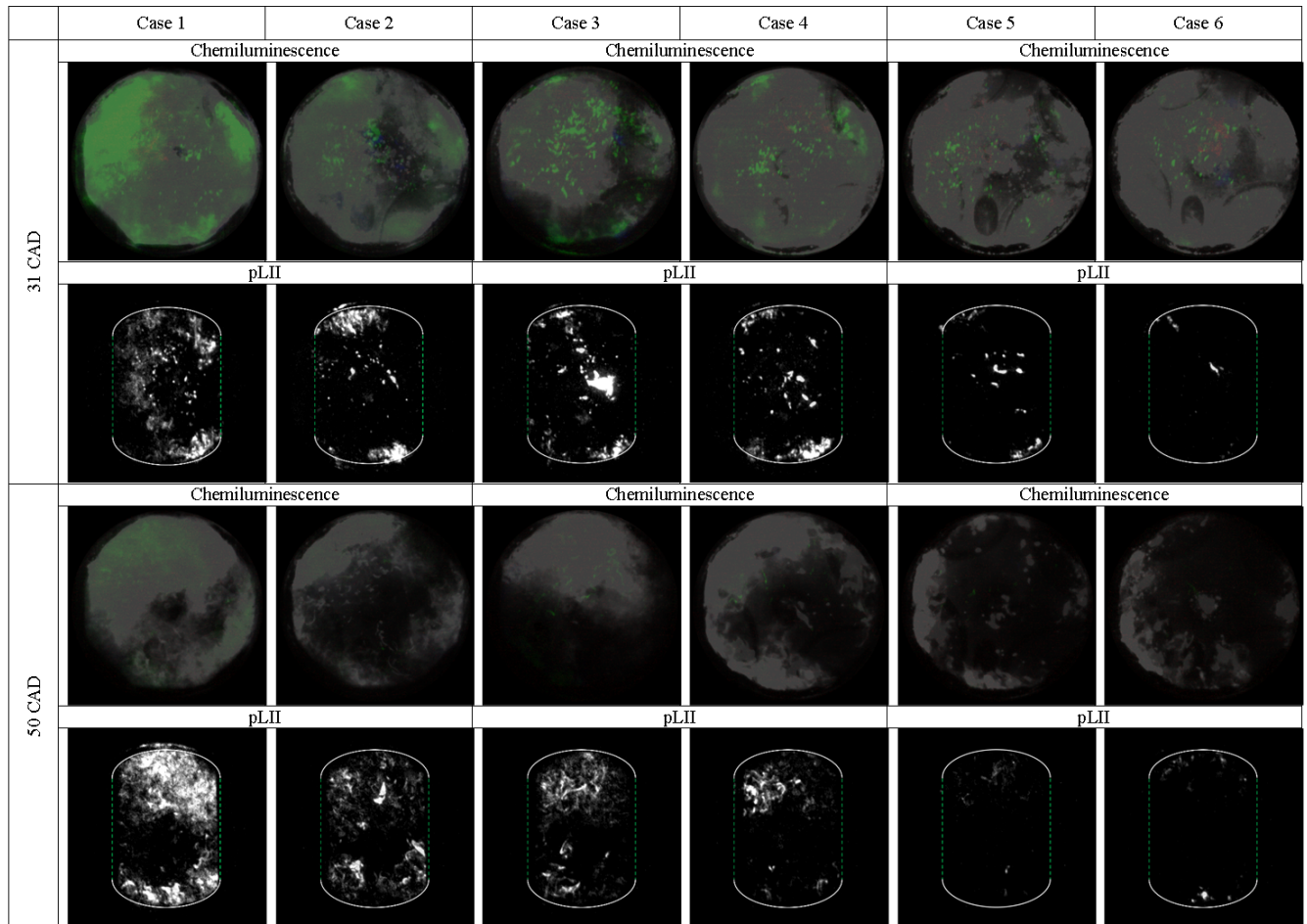
Fig. 19. Spatially integrated pLII signal for all cases considered at 31 and 50 CAD aTDC.